

Inherent Adaptivity of Alzheimer Peptides to Crowded Environments

Silvia De Sio, Jana Waegele, Twinkle Bhatia, Bruno Voigt, Hauke Lilie, and Maria Ott*

Amyloid β ($A\beta$) is the major constituent in senile plaques of Alzheimer's disease in which peptides initially undergo structural conversions to form elongated fibrils. The impact of crowding on the fibrillation pathways of $A\beta_{40}$ and $A\beta_{42}$, the most common peptide isoforms are studied. PEG and Ficoll are used as model crowders to mimic a macromolecular enriched surrounding. The fibrillar growth is monitored with the help of ThT-fluorescence assays in order to extract two rates describing primary and secondary processes of nucleation and growth. Techniques as fluorescence correlation spectroscopy and analytical ultracentrifugation are used to discuss oligomeric states; fibril morphologies are investigated using negative-staining transmission electron microscopy. While excluded volume effects imposed by macromolecular crowding are expected to always increase rates of intermolecular interactions and structural conversion, a vast variety of effects are found depending on the peptide, the crowder, or ionic strength of the solution. While investigations of the obtained rates with respect to a reactant-occluded model are capable to display specific surface interactions with the crowder, the employment of crystallization-like models reveal the crowder-induced entropic gain with $\Delta\Delta G_{\text{fib}}^{\text{crow}} = -116 \pm 21 \text{ kJ mol}^{-1}$ per volume fraction of the crowder.

diseases.^[1] Recent studies, however, have shown that in case of the Alzheimer disease, the loss of synapses and neurons was less strongly correlated to the presence of plaques, but significantly related to the appearance of soluble oligomers of amyloid- β peptides ($A\beta$).^[1–4] Oligomers are aggregates consisting of a few peptides with varying relevance to fibril formation.^[5] Usually, most of the oligomers are in equilibrium with the monomeric peptides rather than being converted into fibrillar species.^[6] Intermediates that ultimately react to form fibrils are prime targets for inhibitory drugs designed to arrest amyloid fibril formation. Hence, molecular insights into the structure and composition of prefibrillar aggregates are essential for the understanding of the overall aggregation process^[7] and toxicity.^[8,9] However, the structural characterization of small aggregates is impeded by their transient nature and their high sensitivity toward environmental changes. Hence, reported oligomers deviate largely in size and in structure. Moreover, the

1. Introduction

The structural flexibility of amyloid peptides comprises the extraordinary property to self-assemble into extended fibrillar structures. Accumulations of fibrillar aggregates, known for the Alzheimer's disease as senile plaques and neurofibrillar tangles, have long been used as hallmarks for neurodegenerative


extremely low concentrations in which $A\beta$ peptides are present in the human body (nanomolar to picomolar range^[10,11]) make it very challenging to track their early stages of aggregation in vivo and has been only succeeded for mice very recently.^[12] Hence, most experiments trying to probe the biophysics of the underlying assembly process are carried out in vitro using dilute solutions. And yet, the intra-cellular and extra-cellular environments are known to be significantly “crowded” with 7% to 40% of the total volume being occupied by a variety of co-solutes and macromolecules^[13–15] making crowding a ubiquitous condition for the natural environment of any protein or peptide in the body.

The main scope of the present study is to investigate the impact of a crowded environments on the pathways of oligomer generation and fibrillation using two of the most abundant $A\beta$ peptides found in amyloid plaques, $A\beta_{40}$ and $A\beta_{42}$, the latter referred as being most toxic.^[16,17] In general, both peptide variants show a very high sensitivity to environmental conditions, like temperature, pH, ionic strength^[18] or concentration^[19] and, most importantly, display different fibrillation mechanisms.^[6] One known difference is the higher hydrophilicity of $A\beta_{40}$. In this study we aim to comparably investigate the consequences of this variation in crowded environments in vitro.

Thermodynamically, amyloid formation originates from an initial supersaturation of amyloid-prone peptides, initiating the formation of β -sheet-rich nuclei, for example, via structural

S. De Sio, J. Waegele, T. Bhatia, H. Lilie, M. Ott
Department of Biotechnology and Biochemistry
Martin-Luther-University Halle-Wittenberg
Kurt-Mothes-Str. 3, Halle, 06120, Saxony-Anhalt, Germany
E-mail: maria.ott@bct.uni-halle.de

B. Voigt
Department of Physics
Martin-Luther-University Halle-Wittenberg
Betty-Heimann-Strasse 7, Halle, 06120, Saxony-Anhalt, Germany

 The ORCID identification number(s) for the author(s) of this article can be found under <https://doi.org/10.1002/mabi.202200527>

© 2023 The Authors. Macromolecular Bioscience published by Wiley-VCH GmbH. This is an open access article under the terms of the Creative Commons Attribution-NonCommercial-NoDerivs License, which permits use and distribution in any medium, provided the original work is properly cited, the use is non-commercial and no modifications or adaptations are made.

DOI: 10.1002/mabi.202200527

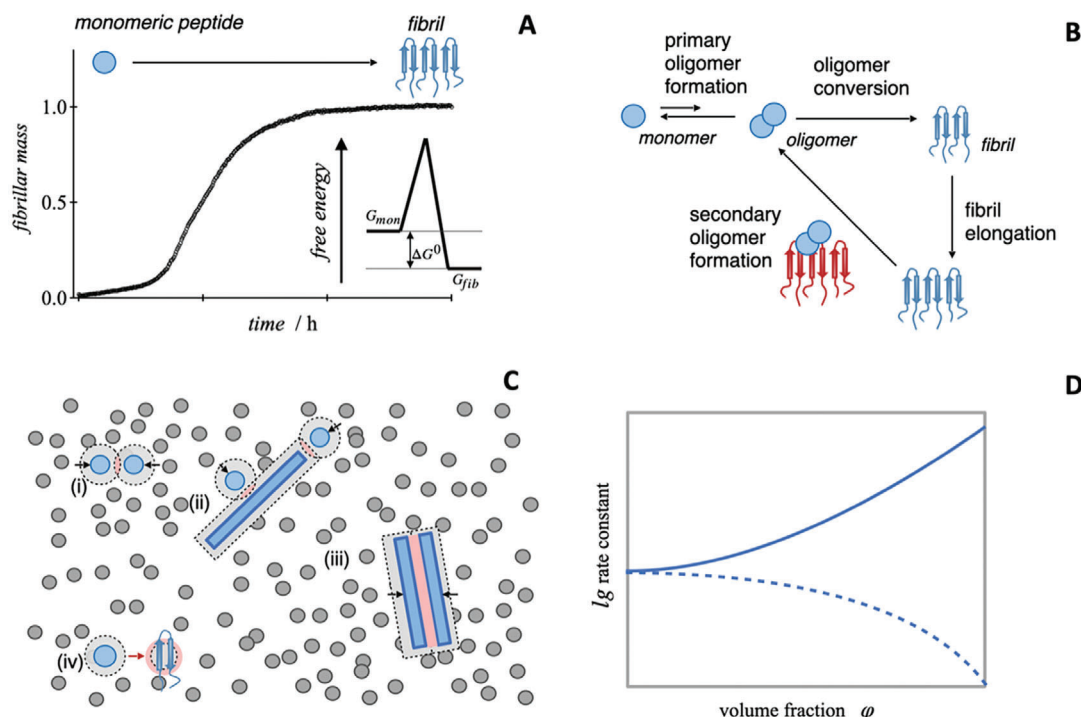


Figure 1. Fibrillation and the impact of macromolecular crowding. A) Fluorescence assays allow to follow the kinetics of fibrillar mass generation with time, $\Delta F(t) \propto \Delta m_{fib}(t)$, with a plateau intensity that also relates to the gain of the Gibbs free energy, ΔG_{fib} . B) Nucleation-and-growth processes can be divided into primary pathways that include the formation of primary oligomers, oligomer conversion and fibril elongation and secondary processes that involve an auto-catalytic cycle of oligomer generation on fibrillar surfaces, oligomer conversion and fibrillar growth. C) Macromolecules may exert depletion forces (black arrows) onto $A\beta$ -peptides (blue) in various stages of its aggregation. The gray shaded areas display regions inaccessible to the centers of mass of the gray spheres (excluded volume). A thermodynamically favorable decrease of the excluded volume may enhance interactions between single peptides or fibrils (i–iii) or support structural conversions, for example, hairpin formation (iv). D) As reaction rate constants of aggregation are usually activation-limited, they are supposed to increase with the crowder's volume fraction, φ (full line). This increase can be impeded by the increase of the solution's viscosity or by occlusion of the reaction surfaces with macromolecules (dashed line).^[37,38]

conversion of preformed oligomers, which then further elongate into mature fibrillar structures by single monomer addition. The amyloidogenic nucleus itself is characterized as a thermodynamically unfavorable species with the highest Gibbs free energy along the reaction coordinate and a structure acting as a seeding template for the subsequent fibrillar growth process.^[20] The latter finally leads to a drop of the free monomer concentration below its critical value of saturation terminating the process of fibrillar growth^[21] (see **Figure 1A**). The gain in fibrillar mass can be understood as a measure for the thermodynamic equilibrium between free monomers and monomers that are incorporated into fibrils.^[22] Notably, fibrillar structures are thermodynamically very stable as they usually display a lower Gibbs free energy as compared to the non-fibrillated peptides. This gain in Gibbs free energy, ΔG_{fib} , was reported to be about 37 and 42 kJ mol⁻¹ for $A\beta_{40}$ and $A\beta_{42}$, respectively.^[23–25]

Moreover, the time-dependence of the fibrillar mass generation obtained from in vitro experiments can be further investigated by recently developed molecular rate-kinetic descriptions of nucleation and growth. This approach allows to discriminate between primary and secondary nucleation pathways.^[5,6] While primary nucleation describes the generation of amyloidogenic nuclei in the absence of fibrils and thus determines the onset of fibrillation, secondary nucleation addresses the auto-cyclic generation of nuclei, for example, via oligomer formation on fibrillar

surfaces (see **Figure 1B**), and thus the ability to amplify amyloid fibrillation.^[26]

High concentrations of non-interacting particles are supposed to impact processes that involve changes of the excluded volume of a system. The excluded volume of a single molecule is the volume that is inaccessible to other molecules (**Figure 1C**). Since the exclusion of accessible volume reduces the configurational entropy of other molecules present in the solution, the Gibbs free energy and chemical potential of each species are thus increased.^[27] Hence, the entropic benefits of dissociated states and unfolded proteins are reduced and equilibria are shifted toward associated states and folded proteins, including self-assembly into stable supramolecular structures as depicted in **Figure 1C(i–iii)** or conformational changes to more compact non-native states (**Figure 1C(iv)**).^[28,29] Moreover, the involved bimolecular rates are supposed to increase by the addition of crowders as assembly processes are usually not diffusion limited (**Figure 1D**). However, hindered diffusion, for example, caging or confinement effects can cause a reduction of the encounter rate at higher crowder concentrations.^[30] Indeed, an overall enhanced fibrillar assembly by macromolecular crowding was predicted^[31,32] and qualitatively observed by experiment, for example, for α -synuclein^[33] or human apolipoprotein C-II.^[34] Up to now, just few experimental investigations on crowding have targeted $A\beta$ peptides. Fung et al.^[35] investigated the effects of

simple saccharides and pointed out that the ability of sugar co-solvents to replace hydrogen-bonded water molecules at peptide surfaces is the most important factor for its interaction with $A\beta$ and that the additional two hydrophobic amino acids associated with $A\beta_{42}$ but not $A\beta_{40}$ are a secondary driving force. In another study, Evgrafova et al.^[36] analyzed the action of thermoresponsive polymers with tunable hydrophobicity on $A\beta_{40}$ fibrillation kinetics, finding out that a higher hydrophobicity corresponded to a kinetic speed-up, while higher hydrophilicity would provoke either a slow-down or no effect at all. These studies are pointing toward the importance of specific crowder interactions, for example, hydrogen bonding, but also less specific hydrophobic interactions. Considering these findings we decided to compare two different model crowders in our study: the linear polymer PEG and the highly branched sugar-based Ficoll molecule.

Here we describe a systematic investigation of the fibrillation kinetics of $A\beta_{40}$ and $A\beta_{42}$ in presence of four different molecular weights of PEG (200, 400, 2'000, and 20'000 g mol⁻¹) and three molecular weights of sugar based polymers (glucose, Ficoll 70, and Ficoll 400). The method chosen to investigate the fibrillation kinetics were fluorescence assays of Thioflavin-T (ThT-assays)^[39] as they allow to monitor the increase of the β -sheet content of an amyloidogenic ensemble with time. We are aware that ThT binding appeared to be sensitive toward parallel β -sheet conformations and early stages are composed of mixtures of parallel and antiparallel β -strands,^[40,41] however, independent of β -strand conformations, the increase in mass of matured fibrils can be reliably monitored.^[42] We further combined the use of ThT fluorescence assays with fluorescence correlation spectroscopy (FCS) to compare the size information obtained from the ThT assays with the average hydrodynamic radii of $A\beta$ in solutions at the early and late stages of fibrillation. FCS was also employed to investigate potential binding of $A\beta$ -peptides to macromolecular crowder molecules. Possible negative effects of crowder molecules on the fibrillation were investigated by transmission electron microscopy (TEM) imaging of the fibril morphologies. Finally, different analytical tools were applied to the ThT assay series to obtain information regarding the preferred pathways of nucleation and growth as well as to reveal enthalpic and entropic effects arising from crowded environments.

2. Results and Discussion

At first we analyzed the fibrillation of pure $A\beta_{40}$ and $A\beta_{42}$ solutions at physiological conditions ($I = 213$ mM, pH 7.4, 37 °C) and dependent on peptide concentrations (2-50 μ M). These investigations allowed us to characterize the individual fibrillation behaviors in terms of the rates of primary and secondary nucleation-and-growth pathways and, most importantly, the sizes of the respective nuclei. The amyloidogenic nucleus is characterized as a thermodynamically unfavorable species with the highest Gibbs free energy along the reaction coordinate and a structure acting as a seeding template for the subsequent fibrillar growth process.^[20]

2.1. $A\beta$ Fibrillation without Macromolecular Crowders

Figure 2A,D displays the averaged ThT-curves for $A\beta_{40}$ and $A\beta_{42}$ solutions at different peptide concentrations together with the

results of the global fits (lines) allowing to determine the concentration dependence of the rates of the primary and secondary pathways, λ and κ , respectively (see Equations (1) and (2)). The trends of the extrapolated fitting parameters, $\lambda(c, \gamma_1)$ and $\kappa(c, \gamma_2)$, where γ_1 and γ_2 are the exponents of the power laws with respect to concentration, c , are depicted as full lines in Figure 2B,E. The latter are compared to a set of parameters λ and κ as achieved by single fitting operations to the same data set using Equation (1) only (symbols). Finally, the parameter A was calculated which is the pre-exponential factor in Equation (1) with $A = \lambda^3 / (3\kappa^3)$.

One of the first results is, that up to peptide concentrations of 10 μ M the parameters obtained from single-curve fitting are very well aligned with the full lines picturing the global fit. This agreement demonstrates that by the reduction of the more complex fitting procedure described elsewhere^[5,43] to Equation (1) with only two fitting parameters λ and κ , allows to reliably untangle primary and secondary pathways of fibrillation even at a single peptide concentration. Above the peptide concentration of 10 μ M though, both rates of $A\beta_{40}$ display a saturation behavior that is well captured by the single-curve fitting procedure, but overlooked by the global fitting as the parameters are forced into following a global power-law dependence with concentration.

A second finding is that the rate describing the secondary pathways, κ , generally exceeds the rate of the primary pathway, λ , for both peptides. This behavior is depicted by the parameter A , that can be understood as a measure of a critical size of the fibrils, at which the auto-catalytic cycles of secondary nucleation sets in [6]. This value is concentration independent for $A\beta_{42}$, while it slightly decreases with concentration for $A\beta_{40}$. The constant behavior in the $A\beta_{42}$ case, is due to the very similar values of both exponents: $\gamma_1 = 0.50$ and $\gamma_2 = 0.43$.

The exponents relate to the description of monomeric nuclei for both, primary and secondary nucleation processes alike, $\gamma_1 = \tilde{n}_1/3$ and $\gamma_2 = (\tilde{n}_2 + 1)/3$ (see Equation (2)), obtaining for $A\beta_{42}$ $\tilde{n}_1 \approx 1.3$ and $\tilde{n}_2 \approx 0.5$. As these numbers are well below two, they signify that already a single $A\beta_{42}$ -peptide is able to form a nucleus by its own through (slow) internal structural conversion. Such a conformational flexibility of $A\beta_{42}$ has been recently described elsewhere by MD simulations^[44] as well as by ssNMR.^[45] In contrast, in the $A\beta_{40}$ case, the decrease of the A parameter with concentration is related to the larger value of the $\gamma_1 = 0.70$ as compared to $\gamma_2 = 0.45$. Making again use of Equation (2), $A\beta_{40}$ displays a dimer as the size of the primary nucleus (with $\tilde{n}_1 \approx 2.1$), while the secondary nucleus again is monomeric (with $\tilde{n}_2 \approx 0.4$). An amyloidogenic $A\beta_{40}$ -dimer has been widely reported being the main fibrillar building block,^[46,47] although none of these studies could address whether the structural conversion to an amyloidogenic structure occurs before or after oligomerization.

In order to address this point for our experimental conditions, we employed experiments of FCS and analytical ultracentrifugation (AUC) to identify possibly abundant oligomeric states. The FCS measurements were carried out on sparsely labeled $A\beta$ peptide solutions, first at high pH 13 and then at pH 7.4. AUC experiments performed under these conditions confirmed that the peptides are monomeric at the high pH (Figure S1, Supporting Information). In accordance, FCS results displayed a hydrodynamic radius, R_h , of 1.1 ± 0.1 nm for $A\beta_{40}$ which is in good agreement with reports of other FCS studies with R_h -values in the range of 0.9 – 1.1 nm for monomeric $A\beta_{40}$ as

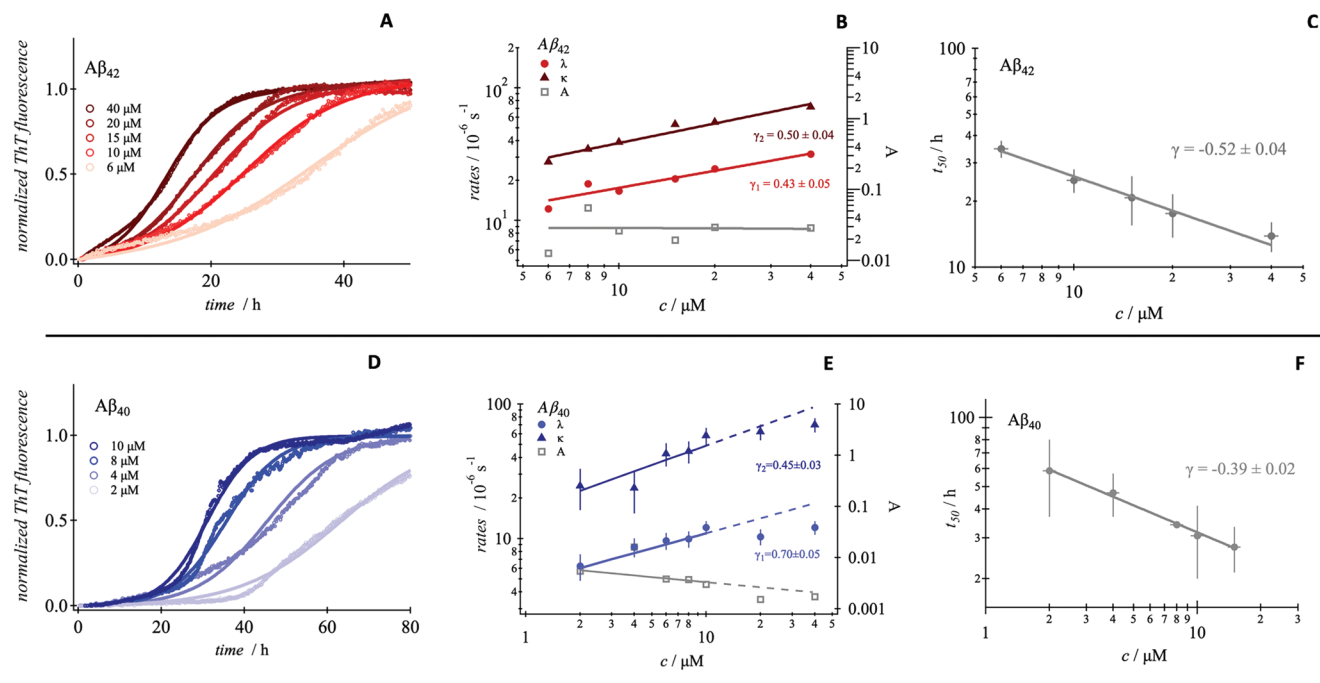


Figure 2. Fibrillation kinetics of $A\beta_{42}$ and $A\beta_{40}$ without crowders. A) Normalized ThT-fluorescence with time of $A\beta_{42}$ and D) $A\beta_{40}$ at different concentrations (symbols) together with the fitting functions (lines) using a global fitting approach (Equations (1) and (2)). B,E) The resulting concentration dependence of the rates for primary and secondary pathways, λ and κ , as well as the growth parameter, A , are displayed as full lines. The global fit results are compared to the means (symbols) and standard deviations (bars) of non-global, individual fits (Equation (1)) for different samples and concentrations. C,F) The concentration dependence of the half times of the fluorescence assays, t_{50} , can be used as an alternative analysis and results in a power-law dependence with exponents of -0.52 and -0.39 for $A\beta_{42}$ and $A\beta_{40}$, respectively. The fibrillation took place at 37°C , near-physiological conditions (pH 7.4, 213 mM ionic strength) and quiescent conditions.

well as $A\beta_{42}$.^[48–50] However, FCS measurements performed at pH 7.4 revealed for $A\beta_{40}$ solutions an apparent radius of $R_h = 1.4 \pm 0.1$ nm, which would rather correspond to a soluble dimer, while $A\beta_{42}$ -solutions stayed monomeric with $R_h = 1.0 \pm 0.1$ nm instead (see Figure S2, Supporting Information). The dimers found in our FCS experiments indicate the presence of a non-amyloidogenic $A\beta_{40}$ entity which eventually may convert into amyloidogenic nuclei. Such a conversion would require coil-to- β -sheet conversions of dimers that were indeed recently described for $A\beta_{40}$.^[51] Moreover and most interestingly, the existence of stable dimers has been predicted for $A\beta_{40}$ only but not for $A\beta_{42}$.^[52,53]

The third set of graphs shown by Figure 2C,F, display the double-logarithmic plots of the half times, t_{50} , which describe the times at which half of the final amount of fibrillar mass has formed in function of concentration. The determination of the power law exponent γ of the relation $t_{50} \propto c^\gamma$ is an established analysis and has often been used to derive information about the nucleus size of the leading fibrillation mechanism.^[54] In our case, assuming the absence of fragmentation due to quiescent fibrillation conditions^[55] and low enough concentrations to avoid saturation effects, secondary nucleation processes are expected to dominate the fibrillation kinetics. Hence, the power-law exponent γ should reveal the bulk nucleus size of secondary nucleation via the equation: $\gamma = -n_2 + 0.5$.^[56] We find n_2 being 1.0 for $A\beta_{42}$ and 0.9 for $A\beta_{40}$, which is in agreement with the analysis discussed above as well as with what has been reported in literature.^[43,56,57]

While the evaluation of the concentration dependence of t_{50} can only display information about the most prominent nucleation mechanism and was used at this point for comparison, the molecular rate-kinetic analysis of Figure 2B,E is in addition able to reveal information about the otherwise hidden primary pathways. This is in particular important as the primary pathway determines the onset of fibrillation. Hence, we will continue with the latter analysis to study the contributions of both rates, λ and κ , for samples at a constant peptide concentration of $10 \mu\text{M}$ and with macromolecular crowders of different molecular weights, chemical composition, structure, and concentrations.

2.2. Effects of Macromolecular Crowding on $A\beta$ -Fibrils

Macromolecular crowding may affect fibrillation in multiple ways. Analyzing fibrillar morphologies can reveal enhancement or inhibition of nucleation as well as crowder-related modifications of fibrillar growth. Similarly, concentration dependent interactions with crowder molecules, not related to excluded volume interactions,^[58] can already be obtained from the plateau intensities of the ThT assays.

Figures 3A and 3G display the fibrillar morphologies of $A\beta_{42}$ and $A\beta_{40}$ in the absence of crowding. For $A\beta_{42}$ we found that the addition of 12% volume fractions of PEG 200 or PEG 2'000 (Figure 3B) did not lead to visibly changes in the fibril

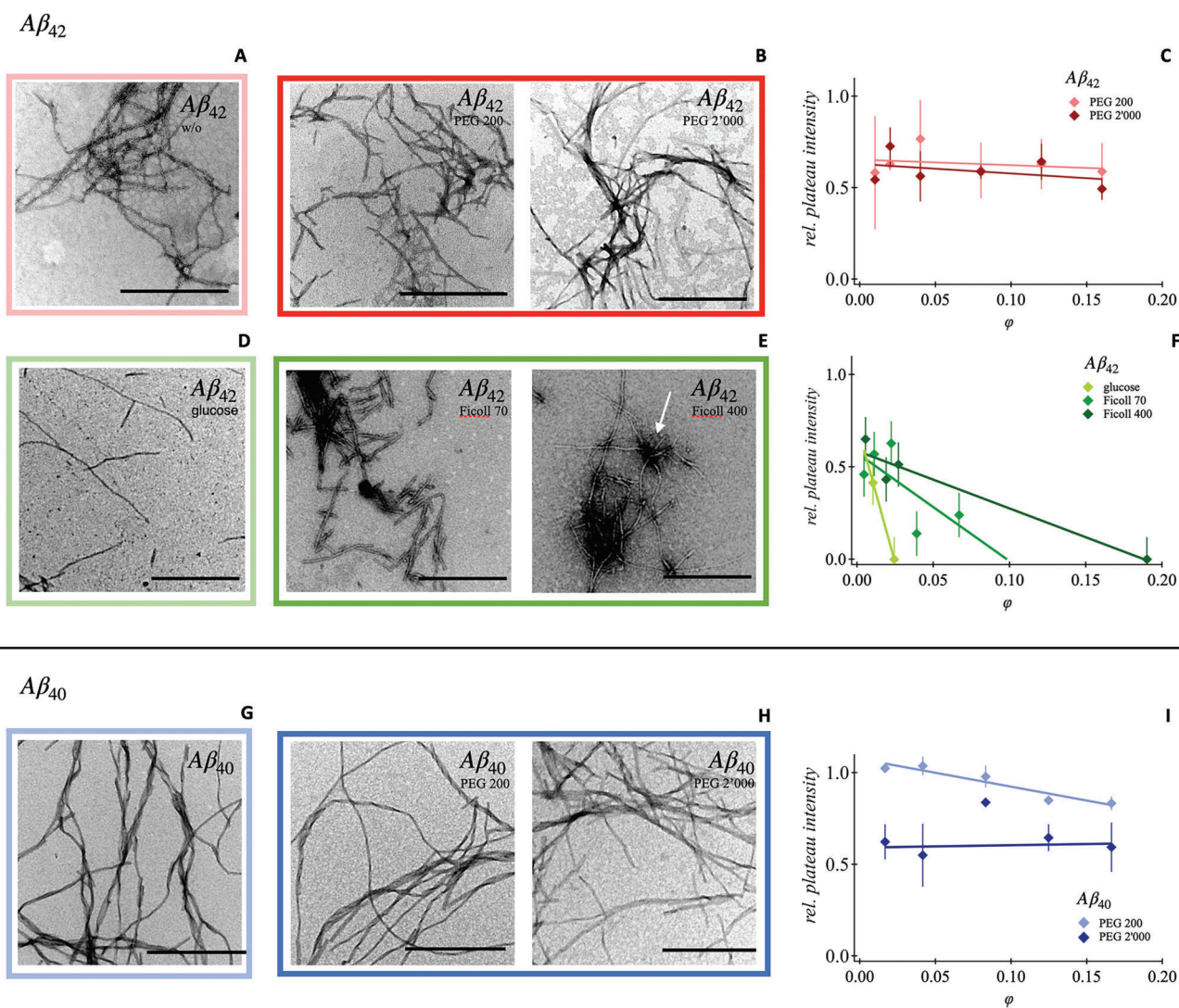


Figure 3. Molecular crowding induced changes on fibril morphology and plateau values of ThT assays. A,C) TEM images of amyloid fibrils of $A\beta_{42}$ and $A\beta_{40}$ in the absence of crowders and B,H) in the presence of PEGs, D) glucose or E) polysaccharides after reaching the final plateaus of fibrillation (after 60–80 h of incubation, see Figures 5 and 6). The volume fractions of the crowders were $\phi = 12\%$ (PEG) and $\phi = 1\%$ (glucose/Ficoll), the scale bars depict 500 nm. C,F,I) The crowder-dependent relative plateau intensities of the fibrillation curves with respect to the plateau values of the crowder-free curves are shown by symbols with standard deviations in the adjacent graphs. The lines are linear fits. All fibrillation processes took place at 37 °C, near-physiological conditions (pH 7.4, 213 mM ionic strength) and in quiescent conditions.

morphology. The fluorescence plateaus though, were reduced by $\approx 40\%$ as compared to the crowder-free case (Figure 3C). The plateau intensities discussed here refer to the ThT assays displayed in Figures 5 and 6 later in the text. The reduction of the plateau values is concentration independent and appears even at very low PEG concentrations. We thus explain this effect either by competitive binding of PEG and ThT molecules to fibrillar surfaces, which is justified by the fact that both molecules are known to bind preferably to hydrophobic sites,^[42,59] or PEG induced changes of the properties of the solution that lead to a change in the ThT fluorescence. Control measurements revealed indeed a similar reduction of the plateau values if PEG 200 or

PEG 2'000 was subsequently added to ThT-labeled $A\beta$ fibrils (see Figure S3, Supporting Information). From the Figures 3D and 3E it is strikingly evident that glucose-based crowders seed $A\beta_{42}$ fibrillation but inhibit fibrillar growth. With glucose (Figure 3D), many very short and premature fibrils were found and in the cases of Ficoll 70 and Ficoll 400 (Figure 3E), dense complexes seem to initiate seeding (white arrow). Moreover, the plateau intensities of glucose and Ficoll solutions (Figure 3F) were strongly reduced with increasing volume fractions, indicating a clear and strong interference with the $A\beta_{42}$ fibrillation process. Hence, Ficolls can not at all be treated as inert crowders. The ability of monosaccharides to hinder $A\beta_{40}$ and $A\beta_{42}$ fibrillation

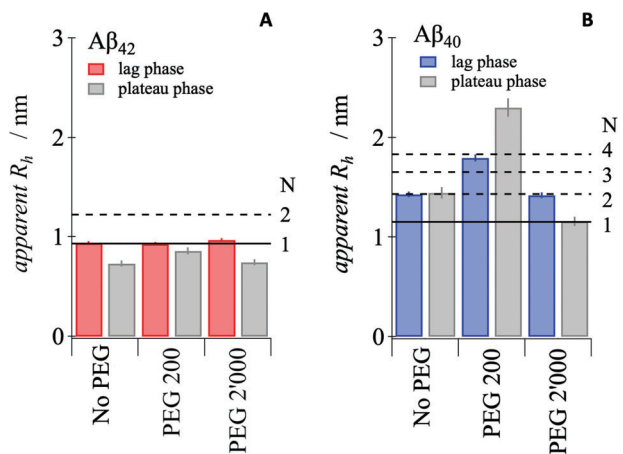


Figure 4. Apparent hydrodynamic radii, R_h , for fluorescently labeled A) $A\beta_{42}$ and B) $A\beta_{40}$ as determined by FCS in different solutions. While the colored bars display the mean values obtained in $10\ \mu\text{M}$ peptide solutions directly after the initiation of fibrillation, the gray bars display the mean values for remaining soluble molecules after 60 h of fibrillation. The values are compared to the monomeric radius, R_h^{mon} , as determined in highly non-fibrillating conditions (black lines), and to the expected values for a spherical N-mer ($R_h^{\text{N}} \approx \sqrt[3]{NR_h^{\text{mon}}}$, dashed lines).

by the formation of stable hydrogen bonds thus increasing native protein stabilities has indeed been reported in literature,^[35] and can, obviously, also be applied to glucose-based polymers such as Ficolls. In contrast, PEG molecules are supposed to increase the hydration of proteins.^[59] Indeed, as for $A\beta_{42}$, the morphologies of $A\beta_{40}$ -fibrils with and without PEG 200 and PEG 2'000 (Figure 3G,H) revealed no significant modifications. Also the plateau intensities with PEG 2'000 were again reduced by $\approx 40\%$ as for $A\beta_{42}$. An exception is made by PEG 200 solutions, where the plateau intensities gradually decrease with increasing PEG concentration.

2.3. Effects of Macromolecular Crowding on the Size of the Soluble $A\beta$ -Oligomer

In order to understand if this behavior might be related to specific binding of crowder molecules also with monomeric $A\beta$, we performed additional FCS measurements with results displayed in Figure 4. Data can be found in the Supporting Information (Figure S4, Supporting Information). For sparsely labeled $A\beta_{42}$ solutions, we could not find an increase of the apparent R_h after the addition of PEG 200 or PEG 2'000 ($\varphi = 12\%$), which would be indicative for binding of PEG molecules to $A\beta$. $A\beta_{40}$ solutions showed, instead, some specific binding to PEG 200 with an increase of the apparent R_h from $1.4 \pm 0.1\ \text{nm}$ (no PEG) to $1.8 \pm 0.1\ \text{nm}$ (12% PEG). With the R_h of PEG 200 being $\approx 0.4\ \text{nm}$,^[60] the increase of the hydrodynamic radius seems indeed indicative for PEG-peptide associations. Such an increase was absent for PEG 2'000. Hence we can conclude, that PEG 200 most probably binds to $A\beta_{40}$ molecules which could also be the reason for the observed concentration dependence of the plateau values shown in Figure 3I. Repeating FCS measurements in the plateau region of the fibrillation, 60 h after the start of the experiment, the apparent R_h of the PEG 200 solution was even further increased (R_h

$= 2.3 \pm 0.1\ \text{nm}$) indicating the formation of stable oligomers that were not consumed by the fibrillation processes. Labeled (proto-) fibrils would be in the range of at least 100 times larger apparent R_h -values^[61] and could be hence excluded. Such a small increase in size was not observed for any other $A\beta$ solution, which rather displayed a constant or slightly reduced apparent R_h . The reduction can be explained by the efficient consumption of monomers, since, tiny amounts of unbound dye molecules ($R_h = 0.6\ \text{nm}$) that originate from the peptide labeling procedure, start to influence the correlation function at very low peptide concentrations ($\approx \text{pM}$).

The evaluation of the fibril morphologies and plateau values of $A\beta$ fibrils using PEGs and glucose-based crowders of different molecular weights allowed three main conclusions: a) the addition of PEG to $A\beta$ solutions did not lead to any significant changes in the appearances of $A\beta_{42}$ and $A\beta_{40}$ fibrils (see Figure 2A,B and G,H); b) the most evident effect of the PEG polymers on $A\beta$ fibril formation being the lowering of the ThT fluorescent intensity by a constant offset (see Figure 2C,I), exception made for $A\beta_{40}$ in combination with PEG 200, which according to our control experiment show a different specific interaction with the peptide (see Figure 2I, light blue); c) glucose-based crowders enhance seeding of fibrils but hinder fibrillar growth even at very low volume fractions of about 1–3% (see Figure 3F) giving rise to multiple shorter fibrils but also a reduced overall fibrillation efficiency (see Figure 3D,E).

2.4. Kinetics of Fibrillation for $A\beta$ Solutions with Macromolecular Crowders

In this section we studied the impact of crowders on the rates for primary and secondary pathways of $A\beta$ nucleation and growth. Figure 5 summarizes exemplary trends of the time-dependent $A\beta_{42}$ -fibrillation with: PEG 200 (A), PEG 2'000 (B), and a summary graph at constant volume fraction $\varphi = 0.12$, but increasing molecular weights (C). These curves are compared to the fibrillation assays with glucose (D), Ficoll 400 (E) and a summary graph at constant volume fraction $\varphi = 0.01$ and increasing molecular weights (F). In each of the aforementioned graphs the black curves indicate the reference fibrillation curves of crowder-free $A\beta_{42}$ at $10\ \mu\text{M}$ peptide concentrations ($I = 213\ \text{nm}$). The lines are fitting functions using Equation (1). The bottom row of Figure 5 summarizes the fitting results obtained for every peptide-polymer solution as compared to the crowder-free case, respectively the same colour code used for the ThT curves.

From the trends shown in Figure 5A we see how the addition of PEG 200 with increasing volume fraction determines an overall retardation of the fibrillation process, whereas the addition of PEG 2'000 shows the opposite trend (Figure 5B), describing a faster fibrillation process with respect to the reference curve. The latter observation is made even clearer by the summary graph Figure 5C, where curves at fixed volume fraction from the $A\beta_{42}$ and PEGs are shown, confirming similar speed-up effects also for the largest PEG used, PEG 20'000 (Figure 5C). This observation is captured by an overall decrease and increase of λ , respectively. Interestingly, secondary nucleation, effects as captured by the rate κ , are reduced for all cases (Figure 5H). In contrast, all curves referring to $A\beta_{42}$ and glucose-based crowders (Figure 5D–F)

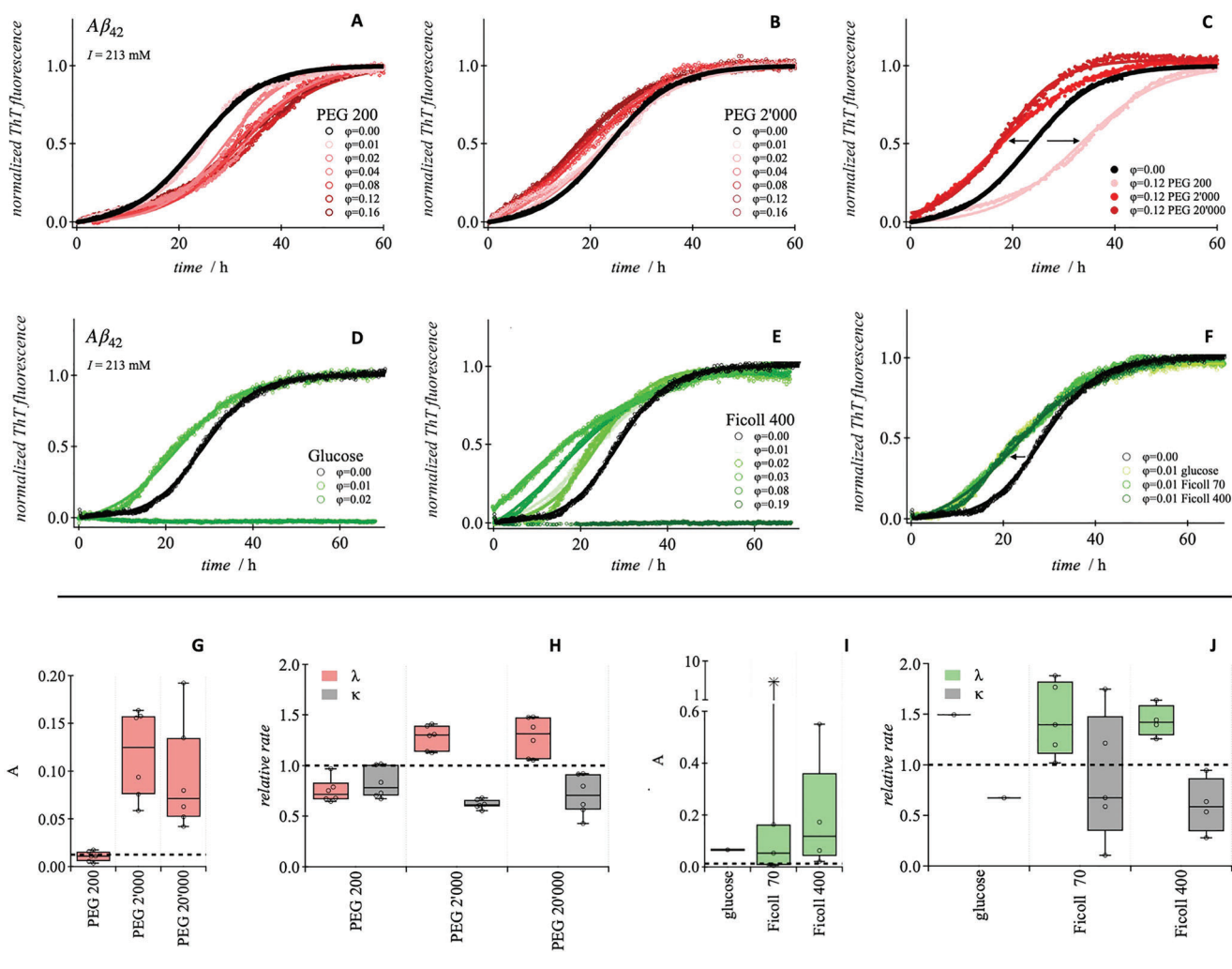


Figure 5. Molecular crowding induced changes of $A\beta_{42}$ fibrillation. Normalized fluorescence assays for $A\beta_{42}$ (10 μ M) mixed with different volume fractions of either A) PEG 200, B) PEG 2'000, D) glucose, or E) Ficoll 400. The assays were averaged and normalized with respect to their plateau values. A comparison of the molecular weight dependence of the fibrillation kinetics are depicted in panel (C) and (F) for PEG and saccharides respectively. Lines display individual fits using Equation (1). The resulting molecular-weight dependence of the fit parameters, λ and κ are depicted for G,H) PEG and I,J) saccharides by using a box and whisker diagram displaying the minimal and maximal values (whisker), lower and upper quartile (box), and median (line) of the crowder concentration series (open circles). The dashed lines display the means of the crowder-free references with $\lambda = (1.4 \pm 0.2) \times 10^{-5} \text{ s}^{-1}$ and $\kappa = (5.0 \pm 0.6) \times 10^{-5} \text{ s}^{-1}$, (mean \pm SD). The fibrillation took place at 37 $^{\circ}$ C, near-physiological conditions (pH 7.4, 213 mM ionic strength) and quiescent conditions.

show a reduced lag time due to the seeding effects proposed earlier. It is worth to notice the smaller volume fractions of sugar-based polymers that already induce a strong impact. At $\phi = 0.01$ (Figure 5D), all curves co-align. The effect of seeding is displayed by an overall increase of λ accompanied by a concentration dependent decrease of κ (Figure 5J). Moreover, the parameter A of panel (I) exceeds 0.5 which is a signature for the change of the sigmoidal shape to a parabolic shape of the ThT curve and an infallible signature for seeding.^[21] Noticeably, in case of the larger PEG crowders, the value of A also increases but stays well below 0.2.

Due to the seeding effects and the inhibition of fibrillar growth in case of glucose, Ficoll 70 and Ficoll 400, the investigation of

these crowders were not continued for $A\beta_{40}$. However, as $A\beta_{40}$ in contrast to $A\beta_{42}$ required dimers to form amyloidogenic nuclei (see Figure 2) and carries a net charge of ≈ -3.2 at pH 7.4, it seemed more meaningful to investigate the fibrillation behavior at lowered ionic strengths of the buffer solutions. Reduced charge screening capabilities of the solvents is expected to enhance the electrostatic repulsion between two peptide molecules. To this respect an analog series of measurements was conducted for $A\beta_{40}$ solutions at a similar ($I = 213 \text{ mM}$) and at a lower salt concentrations ($I = 78 \text{ mM}$). Figure 6 shows the averaged ThT-curves of $A\beta_{40}$ in two different buffers and with increasing PEG 200 (A,D) and PEG 2'000 (B,D) volume fractions, and a summary graph of all molecular weights at a fixed volume fraction (C,E).

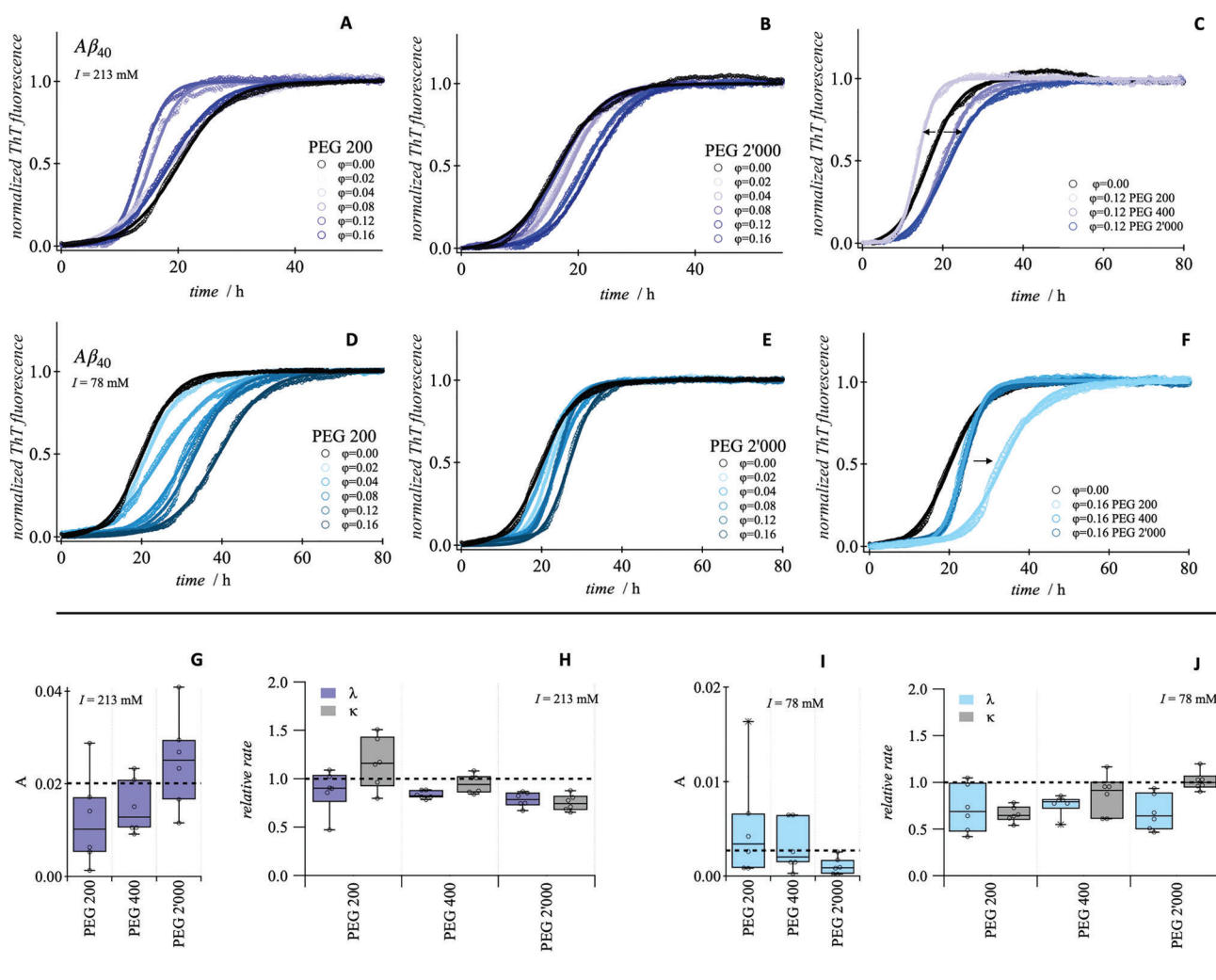


Figure 6. Molecular crowding induced changes of $A\beta_{40}$ fibrillation. Normalized fluorescence assays for $A\beta_{40}$ ($10 \mu\text{M}$) mixed with different volume fractions of either A, D) PEG 200, B, E) PEG 2'000 for physiological (213 mM) and low (78 mM) ionic strengths. A comparison of the molecular weight dependence of the fibrillation kinetics are shown in panels (C) and (F). Lines display individual fits using Equation (1). The resulting molecular-weight dependence of the fit parameters, A , λ , and κ are depicted by using a box and whisker diagram (G–J) displaying the minimal and maximal values (whisker), lower and upper quartile (box) and median (line) of the crowder concentration series (open circles). The dashed lines display the means of the crowder-free references with $\lambda = (2.6 \pm 0.5) \times 10^{-5} \text{ s}^{-1}$ and $\kappa = (6.6 \pm 0.1) \times 10^{-5} \text{ s}^{-1}$ for $I = 213 \text{ mM}$ (G, H) and $\lambda = (1.7 \pm 0.3) \times 10^{-5} \text{ s}^{-1}$ and $\kappa = (8.3 \pm 0.2) \times 10^{-5} \text{ s}^{-1}$ for $I = 78 \text{ mM}$ (I, J), (mean \pm SD). The fibrillation took place at 37°C , pH 7.4, and quiescent conditions.

The black curves always indicate the reference fibrillation curves of pure $A\beta_{40}$ solutions, and the lines display the fitting functions obtained using Equation (1). The third row sums up the fitting parameter A , λ and κ for the aforementioned cases.

Comparing at first the impact of PEG crowders on $A\beta_{40}$ and $A\beta_{42}$ fibrillation at the higher ionic strength, the exact opposite trends for the two rates were discovered. While solutions of $A\beta_{42}$ and PEG 2'000 displayed a speed-up of fibrillation with respect to the reference curve, $A\beta_{40}$ and PEG 2'000 solutions showed a slow-down. The opposite was true for PEG 200. Comparing the evaluated fitting parameters as obtained for $A\beta_{40}$ and $A\beta_{42}$ (Figures 6H or 5H), one finds for PEG 2'000 that the enhanced fibrillation in case of $A\beta_{42}$ is mainly due to an increase of the rate

of the primary pathway, λ ; while the latter is reduced for $A\beta_{40}$. κ is reduced in both cases. PEG 200, however induced a reduction of both rates for $A\beta_{42}$, while for $A\beta_{40}$ only λ was reduced, but κ enhanced. The differences for κ might origin from different interactions of PEG with each of the fibrillar surfaces as bound PEG molecules may hinder or enhance secondary processes on fibrillar surfaces. Interestingly enough, lower ionic strengths led for $A\beta_{40}$ to a further overall reduction of both rates, λ and κ , which can be explained by stronger intermolecular repulsion. Contrary, in case of PEG 2'000, only λ was reduced. These highly different responses led to the question by which molecular mechanism macromolecular crowders are able to influence the pathways of primary or secondary nucleation.

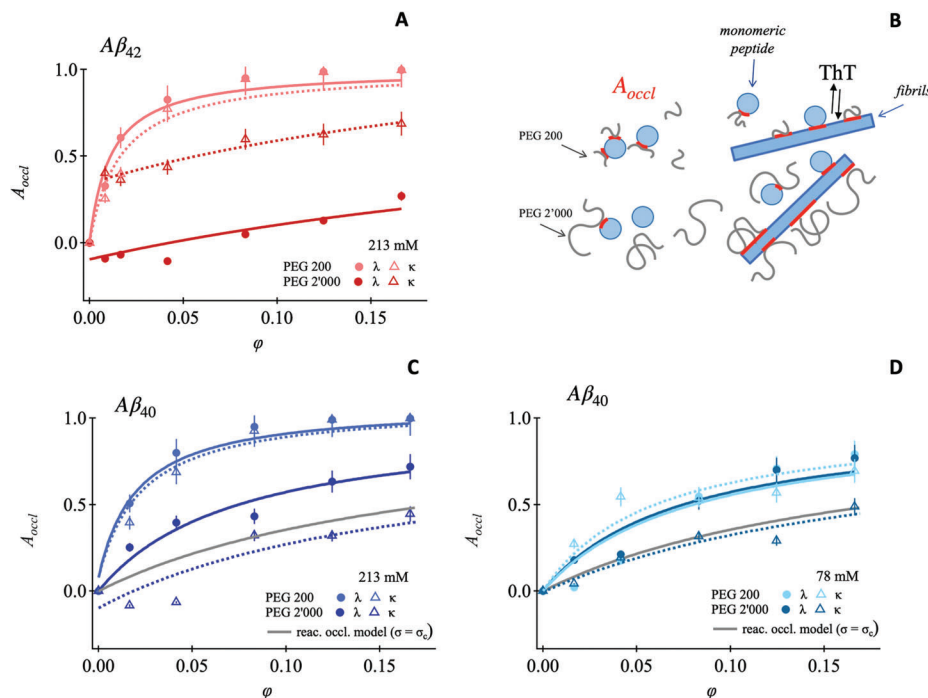


Figure 7. Reactant occlusion. Relative occluded surface areas of solutions of A) $A\beta_{42}$ and C,D) $A\beta_{40}$ with respect to the volume fractions of PEG 200 and PEG 2'000 as received from $\lambda(\varphi)$ and $\kappa(\varphi)$ using Equation (6). The lines describe the fits according to Equation (8). The concept of occluded surfaces is schematically depicted in (B) with the temporarily occluded areas marked red.

2.5. Reactant Occlusion through Macromolecular Crowding

In order to further investigate the impact of PEG molecules on both fibrillation pathways, we applied a reactant-occlusion model that describes possible effects of crowders that do not bind permanently, but are able to exclude accessible surface areas from interacting peptides, for example, by spatial separation of two molecules thus slowing down the reactions rates (red areas in **Figure 7B**). The applicability of this model function was ensured as our fibrillation rates were all found to be within the activation limit (see theory section for the mathematical background). At first, we applied Equation (6) to the rates $\lambda(\varphi)$ and $\kappa(\varphi)$ of the data sets displayed in Figures 6 and 5 to obtain the respective relative occluded areas, $A_{occl}(\varphi)$, with increasing volume fraction of the crowder (data points of **Figure 7A,C,D**). In a second step, we applied a quantitative analysis to the obtained data sets by fitting $A_{occl}(\varphi)$ with Equation (8) as a fitting function (lines). The latter, as it has been derived for spherical particles, provides a single fitting parameter, ρ_C , describing the apparent radius of the molecule causing the effect of volume occlusion. Interestingly, we found in PEG 200 solutions for the primary pathways of both peptides a very similar result, with $\rho_C = 0.31 \pm 0.04$ nm and $\rho_C = 0.37 \pm 0.06$ nm for $A\beta_{42}$ and $A\beta_{40}$ respectively (**Figure 7A,B**). For the secondary processes in the presence of PEG 200, again, all values were very similar with 0.38 ± 0.05 and 0.39 ± 0.06 nm for $A\beta_{42}$ and $A\beta_{40}$, respectively. As this size range is comparable to the R_h of PEG 200 with ≈ 0.4 nm,^[60] we can conclude that PEG 200 molecules indeed occlude reactant surfaces for primary and secondary processes alike.

For solutions with PEG 2'000, these findings deviate. While one finds large differences for $A\beta_{42}$ with $\rho_C = 1.57 \pm 0.33$ nm

(λ) and $\rho_C = 0.55 \pm 0.06$ nm (κ), $A\beta_{40}$ displays the opposite trends with $\rho_C = 0.69 \pm 0.09$ nm (λ) and $\rho_C = 0.98 \pm 0.04$ nm (κ). In addition there are negative and positive offsets, as seen for both of the peptides in **Figure 7A,B**, hinting toward crowder-independent contributions from the system. As R_h of PEG 2'000 is ≈ 1.3 nm,^[60] this size would only match ρ_C as determined for the primary process of $A\beta_{42}$ and does not explain the size range of 0.6–0.9 nm. However, the only particles of that size that are omnipresent in the sample is the $A\beta$ peptide itself. Hence, it might be possible that PEG molecules also stabilize transient binding of $A\beta$ peptides, leading to an apparent occlusion of binding sites as the majority of the bound peptides do not convert into seeds. Such an effect would strongly depend on the charge screening properties of the solutions, as the peptides are negatively charged. Weak binding of $A\beta$ -peptides should become even weaker at lower ionic strengths. Indeed, we did not find any offset at low ionic strengths, but similar apparent “crowder” sizes with ρ_C of 0.67 ± 0.09 nm (λ) and 0.58 ± 0.05 nm (κ) for PEG 200, and 0.64 ± 0.06 nm (λ) and 1.08 ± 0.09 nm (κ) for PEG 2'000 (**Figure 7D**). Hence we conclude that in case of PEG 200 and high ionic strengths, the volume occlusion is driven by the crowder molecule alone, while a combination of PEG and peptide interactions appear for PEG 2'000 at high and at low ionic strengths.

2.6. $A\beta_{42}$ Fibrillation at Low Ionic Strengths with PEG Crowders

The discussion of the last part imperatively leads to the question, whether even the very weak enthalpic interactions of PEG always dominate the Gibbs free energy contributions or if conditions could be found to also reveal entropic contributions from the

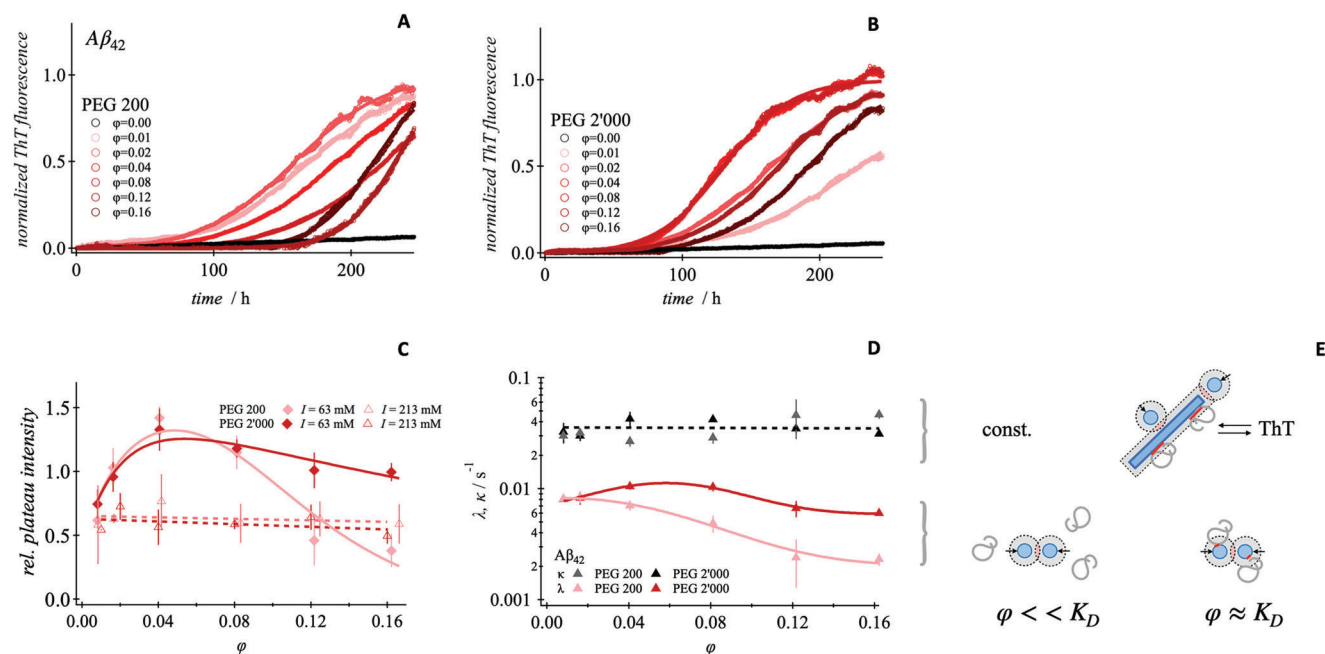


Figure 8. Molecular crowding induced changes of $A\beta_{42}$ fibrillation at low ionic strengths. Normalized fluorescence assays for $A\beta_{42}$ (10 μM) mixed with different volume fractions of either A) PEG 200 or B) PEG 2'000. The assays were averaged and normalized with respect to their (fitted) plateau values. Lines display individual fits using Equation (1). C) Relative plateau intensities of $A\beta_{42}$ solutions with PEG 200 and PEG 2'000 for $I = 63$ mM (closed symbols) and $I = 213$ mM (open symbols) with respect to the mean plateau value of the crowder-free reference. The solid lines display fits using Equation (12). The rates λ and κ derived for PEG 200 and PEG 2'000 using Equation (1) are displayed in (D) together with a scheme depicting the possible interactions of $A\beta_{42}$ with PEG and ThT for the rates κ (E, top) and λ (E, bottom). The fibrillation took place at 22 $^{\circ}\text{C}$, pH 7.4, 63 mM ionic strength and quiescent conditions.

crowded environment, as discussed in the introduction (see Figure 1). In order to address this question, we selected $A\beta_{42}$ as it nucleates efficiently from a monomer and hence does not need another peptide molecule to form its primary nucleus (Figure 2A). Moreover, $A\beta_{42}$ did not form the larger oligomers with PEG 200 (see Figure 4) and its primary nucleation seems to be the least affected by volume occlusion effects (see Figure 7A). Hence, we assume much lower enthalpic interactions with PEG molecules as compared to $A\beta_{40}$. $A\beta_{42}$ fibrillation experiments were thus performed at even lower ionic strengths than previously described for $A\beta_{40}$. Under these conditions, $A\beta_{42}$ solutions did not fibrillate without the assistance of crowders within the time frame of 150 h, while even the lowest concentrations of PEG of any size could induce fibrillation. Unfortunately, the data obtained at 37 $^{\circ}\text{C}$ displayed a weak second fibrillation component which would hamper the evaluations of the kinetics of the fibrillation (Figure S5, Supporting Information). Hence, we decided to reduce the temperature to room temperature to suppress this weak component, which was successful.

Figure 8 displays the results for the fibrillation of $A\beta_{42}$ at increasing volume fractions of PEG 200 and PEG 2'000 (A,B). The first obvious difference in comparing the results to previous experiments is the modulated lag times that seem to initially shorten with increasing volume fractions and then, after an optimum is reached, to decrease again. For comparison, while the optimum volume fraction for PEG 200 was reached at $\varphi = 2\%$, PEG 2'000-solutions displayed their optimum at about $\varphi = 8\%$. This feature was also captured by the variations of the plateau intensi-

ties (Figure 8C) and rates of primary nucleation and growth (Figure 8D). Notably, the rate for secondary processes was not influenced by the crowder molecules and was remaining almost constant.

Comparing the obtained plateau intensities with those measured at the higher ionic strength, the latter all converged to the same value at low volume fractions. This indicated that the competitive binding of ThT and PEG was comparable for both solutions at low PEG concentrations and the observed variations of the plateau intensities are proportional to the fibrillar mass and to a possible recruitment of ThT binding sites by PEG molecules as derived in the theory's section. Applying Equation (13) to our experiments (lines in Figure 8C), we could deduce three parameters from the fit: a slope m that describes the proportionality $\Delta\Delta G_{\text{fibril}}(\varphi) = m\varphi$ and the parameter set K_d and n describing the binding of PEG molecules. While the latter were determined to be $K_d = 43 \pm 4$ g L^{-1} and $n = 3.2 \pm 0.1$ for PEG 200 and $K_d = 16 \pm 8$ g L^{-1} and $n = 1.3 \pm 0.7$ for PEG 2'000, the slope was fitted globally for both PEG sizes and was determined as $m = 116 \pm 21$ kJ $\text{mol}^{-1} \varphi^{-1}$. The conclusions from these results are, i) the interactions of PEG molecules with $A\beta$ do not scale linearly with the number of chain ends per volume, but are also size dependent. The latter is depicted by the parameters K_d and n that do not simply relate to the number concentration. ii) More importantly, the reduction of the interparticle interactions of PEG and $A\beta$ by lowering the ionic strength of the solution, finally allowed to reveal and analyze the PEG-induced gain in entropy for $A\beta_{42}$ fibrillation.

3. Summary and Conclusions

In this study we investigate the impact of crowder molecules on the fibrillation of $A\beta_{40}$ and $A\beta_{42}$. The general fibrillation mechanisms of the peptides in the absence of crowders were characterized in the case of $A\beta_{40}$ by primary nucleation via structured dimers, whereas $A\beta_{42}$ fibrillation was initiated by internal conversion of a monomer. Both peptides showed an overall dominance of secondary nucleation. After these investigations we moved on to study the addition of PEGs, glucose and Ficoll with varying molecular weights and volume fractions up to 20%. While Ficoll and glucose induced seeding and hampered fibrillar growth, we found that PEG molecules do not change the morphologies of the fibrils. In detail investigations of the fibrillation kinetics of the two peptides with PEG, however, did not reveal a consistent acceleration of the two investigated rates of primary and secondary nucleation pathways as expected for excluded volume effects. While the addition of PEG 2'000 enhanced the rate for the primary pathway of $A\beta_{42}$, a reduction of this rate was observed for PEG 200. A similar diametrically opposite response to PEG 200 was observed between $A\beta_{40}$ and $A\beta_{42}$ regarding their secondary pathways. This finding may go along with the higher hydrophobicity of $A\beta_{42}$ which makes it more prone for secondary processes and seeding (heterogeneous nucleation).^[62] The latter seemed to be promoted by the presence of Ficolls as possible nucleation-active surfaces. Contrary, the higher hydrophilicity of $A\beta_{40}$ may be the reason for the overall enhanced homogeneous nucleation in solutions without crowders and may also cause the reduction of the rates of the primary pathways of fibrillation in the presence of PEG molecules.

At near-physiological conditions, secondary processes were mostly retarded (especially for PEG 2'000) and we concluded that surface effects, for example, coverage of fibrillar surfaces by PEG molecules or trapped peptides may play a crucial role. At low ionic strengths, this effect is reduced which could be confirmed by experiments in which PEG was subsequently added to a fibrillated solution. Yet, the reduced electrostatic screening also slowed down the rate of the primary nucleation leading again to a balanced situation between the rates of primary and secondary processes.

The phenomenon of the possible interactions of PEG with fibrillar surfaces was further studied by employing a reactant occlusion model to the kinetics of the primary and secondary processes of $A\beta$ fibrillation. This model allowed, for example, to relate the enhanced rates of the primary pathway of $A\beta_{42}$ with PEG 2'000, to a low occluded area, while the reduced rate of secondary nucleation was related to a highly occluded reaction area. $A\beta_{40}$ displayed the opposite behavior. Hence, we could confirm, that even weak or transient interactions and spatial hindrance effectively reduces the rates of fibrillation in a macromolecular crowded environment. This effect was strongly related to the sizes of the crowders but was also pathway dependent. Moreover, we found a hint for possible self-crowding of $A\beta$ peptides blocking binding sites for secondary oligomer generation. With these findings we can conclude that even with the least interacting crowder (PEG), enthalpic contributions steered the rates of fibrillation making entropic contributions invisible. Just a reduction of these weak interactions by choosing different experimental conditions could

reveal the promoting role of excluded volume interactions on $A\beta$ fibrillation.

We can hence conclude that in crowded environments, such as live cells, excluded volume interaction would most probably not enhance the fibrillation kinetics of both of the $A\beta$ peptides despite of their differences in terms of hydrophobicity and sizes of the primary nuclei. The weak and possibly transient interactions of crowder molecules with the fibrillar surfaces allow the system to modulate the efficiency of secondary fibrillation pathways. These findings need to be carefully considered if surface sensitive experimental techniques as ThT-assays are applied or in vitro experiments display enhanced secondary nucleation. Secondary processes of the same molecule in a cellular context might be much less dominant compared to in vitro observations.

4. Experimental Section

Materials: $A\beta_{40}$, $A\beta_{42}$ as well as the N-terminal labeled $A\beta$ -variants (Atto488- $A\beta_{40}$, Atto488- $A\beta_{42}$) were synthesized by the Core Unit of Peptides-Technologies of the University of Leipzig using microwave-assisted solid-phase peptide synthesis (CEM GmbH, Germany) based on Fmoc-strategy. The fluorescent marker Atto488 was received from Atto-TEC GmbH, Germany. PEG 200, PEG 400, PEG 2'000, PEG 20'000, glucose, Ficoll 70, and Ficoll 400 were purchased from Sigma-Aldrich (Merck KGaA, Germany).

Methods: The impact of macromolecular crowders on the fibrillation of $A\beta_{42}$ and $A\beta_{40}$ was investigated using ThT-fluorescence assays of four to six different concentrations for each selected macromolecular crowder and buffer condition. For each data point at least three fluorescence assays were measured and averaged prior to data analysis. The calculation of the overlap concentration of the crowder molecules can be found in the Supporting Information (Section S1.1, Supporting Information).

Sample Preparation: $A\beta$ peptides were first dissolved in a crowder-free, 60 mM sodium-hydroxide solution at pH 13 to ensure monomeric starting conditions (Figure S1, Supporting Information). The final pH value of 7.4 and the final peptide concentration of 10 μ M was achieved by adding a 25 mM sodium-phosphate buffer of pH 6.0. The second buffer contained the necessary amount of sodium chloride and polymers to achieve the final total ionic strengths, I , of 63, 78, or 213 mM and the desired crowder concentrations. Each polymeric suspension was prepared by dispersing 1 M concentration in and then left to stir overnight to ensure full hydration of the dispersed polymers. From these stock solutions, the desired concentrations used in the measurements were freshly diluted shortly before each measurement. All $A\beta$ -peptide solutions were freshly prepared and always immediately used after preparation. Samples were prepared from the peptides and polymers stock solutions directly in the 150 μ L volumes of the well-plate-reader wells.

Negative-Stain Transmission Electron Microscopy (TEM): 5 μ L of the fibrillated sample was transferred to a 200-mesh copper grid coated with a Formvar/Carbon film and incubated for 3 min. After removing the supernatant, the grid was washed with ddH₂O and subsequently stained with 1% uranyl acetate for 1 min. The grid was allowed to dry for 24 h on filter paper after removing excessive uranyl acetate solution. Imaging was conducted on a Zeiss EM900 microscope at 80 kV acceleration voltage in transmission mode.

ThT-Fluorescence Assays: 2.5 mM Thioflavin T (Sigma Aldrich, Germany) stock solution, prepared in pure deionized water (MQ-water), was stored at 4 °C in the dark. Directly before the measurements it was filtered through a 0.2 μ m filter and diluted 1:10 in a 25 mM phosphate buffer of pH 7.4. Of the latter a total volume of 3.6 μ L was added to 146.4 μ L of the peptide solution to reach a total volume of 150 μ L for each well with a final ThT concentration of 20 μ M. The addition of this small amount of ThT solution was well considered in the fibrillating solutions' final ionic strength and polymer concentration determination. The samples were incubated

in 96-wells PEG-coated black polystyrene plates with clear bottoms (Corning 3881, Massachusetts, USA) at 37 °C under quiescent conditions and their aggregation kinetics, studied with a FluoStar Omega well-plate reader (BMG Labtech, Offenberg, Germany) with measurements of the ThT-fluorescence intensity as a function of time set every 300 s, using 440 nm wavelength as excitation and 480/10 nm for detection. The time dependencies of the ThT fluorescence were analyzed by calculation of the average ThT fluorescence of at least three measurements and applying the fitting function of Equation (1) to the averaged ThT curve. An exception was made for the concentration series of $A\beta_{40}$ or $A\beta_{42}$ in the absence of crowders. In this case, individual fits and subsequent calculation of the mean and standard deviation was used as well as a global fitting approach combining Equations (1) and (2). The exponents \tilde{n}_1 and \tilde{n}_2 were derived by applying a linear fit to a plot displaying the logarithms of the rates, $\log(\lambda)$ and $\log(\kappa)$, versus the logarithms of the concentrations, $\log(c)$. The same procedure applied to the concentration dependency of t_{50} , for which the slope of $\log(t_{50})$ versus $\log(c)$ was fitted to determine γ . The curves were normalized according to the fitted plateau values using Equation (1).

Analytical Ultra-Centrifugation (AUC): $A\beta_{40}$ and $A\beta_{42}$ were analyzed at protein concentrations of 200 μM in 60 mM NaOH, pH 13 in a Beckman Optima XL-I centrifuge equipped with an An50Ti rotor and double sector cells. Sedimentation measurements were carried out at 20 °C and 40 000 rpm. For sedimentation velocity data were recorded every 10 min in the first 5 h, afterward every 60 min for additional 10 h. Sedimentation equilibrium was reached after ≈ 60 h. The data were monitored in a wavelength range of 230–280 nm and analyzed using the software Sedfit.^[63]

Fluorescence Correlation Spectroscopy (FCS): FCS measurements of $A\beta_{40}$ or $A\beta_{42}$ were carried out on sparsely labeled samples at concentrations of 10 μM (degree of labeling $< 0.02\%$). Up to a degree of labeling of 5%, the selected fluorescent marker Atto488 was previously reported to not effect the fibrillation kinetics nor fibril morphologies of the $A\beta$ -peptides.^[64] Within the time frame of the FCS measurements (15–30 min), no larger fluorescence fluctuations with dwell times above 100 ms as indicative for the diffusion of protofibrils or fibrils,^[61] were observed. Experimental details of the FCS setup and data analysis can be found in the Supporting Information (Section S1.2, Supporting Information).

Determination of the Rates of Primary and Secondary Pathways, λ and κ : The time-dependent increase of the ThT-fluorescence by the function was analyzed.^[6]

$$\Delta F(t) = \left(1 - \frac{1}{\frac{\lambda^3}{3\kappa^3} (e^{\kappa t} - 1) + 1} \right) \Delta F_{\text{plateau}} + a \cdot t \quad (1)$$

where λ and κ refer to primary and secondary pathways of fibrillation,^[43] respectively, and the parameter a describes a apparent slope that accounts for a slightly increasing plateau value. The latter was required for $A\beta_{40}$ at high ionic strengths only, and was zero otherwise. Within the model description of Equation (1), the rates λ and κ comprise individual microscopic rates of oligomerization, structural conversion, and elongation. Since it was focused in the study on the interplay between primary and secondary pathways it is sufficient to determine the overall rates λ and κ as previously shown in ref. [65]. In addition, a characterization of the concentration dependence of both rates allowed to extract information about the microscopic sizes of the nuclei of each pathway, \tilde{n}_1 and \tilde{n}_2 , using the relations^[5,6]

$$\begin{aligned} \lambda &\propto m_{\text{mon}}^{\tilde{n}_1/3}, \\ \kappa &\propto m_{\text{mon}}^{(\tilde{n}_2+1)/3} \end{aligned} \quad (2)$$

where m_{mon} refers to the total mass of monomers and scales with the concentration. \tilde{n}_1 and \tilde{n}_2 derive from rate equations for oligomer-mediated fibrillation. They described the reaction orders of the primary and secondary nucleation pathway, including oligomerization and structural conversion.^[6] The reaction order was further related to the oligomeric

size (number of monomers) of an amyloidogenic nucleus allowing subsequent fibrillar growth.

Effect of Macromolecular Crowding on Microscopic Rates: Macromolecular crowding induced at least two major opposing effects on the reaction rates of proteins.^[37] While on the one hand the reduction of the available volume was expected to lead to an increase of the collision rates of the reactants due to their increased effective concentration within the reduced available volume, on the other hand, macromolecules might inhibit peptide diffusion and thus leading to an effective reduction of reaction rates (see Figure 1D). A kinetic description of the impact of excluded volume effects on a microscopic rate of interacting particles, $k(\varphi)$, was developed by Berezhkovskii and Szabo.^[66] In the absence of non-specific binding to crowder molecules, the rate constant could be expressed by the modified Collins–Kimball formula

$$\frac{1}{k(\varphi)} = \left[\frac{1}{k_0} + \frac{1}{4\pi D(\varphi)\rho_{AB}} \right] \exp^{-\Delta G/k_B T} \quad (3)$$

where k_0 is the intrinsic or reaction-controlled rate constant, $D(\varphi)$ the relative diffusion coefficients of the reactants and ρ_{AB} the sum of the radius of the interacting particles A and B, $\rho_{AB} = \rho_A + \rho_B$.

The gain of the Gibbs free energy for crowded systems, $\Delta G_{\text{crow}} = \Delta U_{\text{crow}} - T\Delta S_{\text{crow}}$, included enthalpic (ΔU) and entropic (ΔS) contributions. ΔU_{crow} could be described by a crowder-induced potential well localized in the depletion zone,^[66] but should be neglected in the following ($\Delta U_{\text{crow}} \approx 0$). The change in entropy can be written as

$$\Delta S_{\text{crow}}(\varphi) = \ln(1 - \varphi_x(\varphi, \tilde{\rho}))/T \quad (4)$$

with φ_x being the fraction of the system's volume excluded to the particle and given by the empirical equation $\varphi_x = \varphi_x(\varphi, \tilde{\rho}) \approx 1 - \exp[-\varphi(\tilde{\rho} + 1)^3 - \varphi^2(16.4\tilde{\rho}^2 + 5.31\tilde{\rho} + 0.474)]$.^[38] The tilde symbol implies a reduced radius in which ρ is divided by the crowder radius, ρ_C , with $\tilde{\rho} = \rho/\rho_C$. If macromolecules did not only occupy volume but also exclude reaction surfaces from the reactants, for example, by spacial separation of two reactants, $k(\varphi)$ would be reduced by the fraction of the occluded area, A_{occl} . This reduction would in case of activation-limited reactions be directly proportional to the relative exposed effective surface area^[38] and

$$k(\varphi) \propto 1 - A_{\text{occl}}(\varphi) \quad (5)$$

A criterion to differentiate whether a reaction is diffusion-limited or activation-limited was given by the ratio $\gamma = k/4\pi D(\varphi)\rho_{AB}$, which is 1 for diffusion-limited processes and 0 for pure activation-limited reactions. It was found that the crowding experiments were activation-limited with $\gamma < 3 \times 10^{-6}$. Finally, including $S_{\text{crow}}(\varphi)$ of Equation (4) and the occluded-area effects of Equation (5) into Equation (3), the reactant-occluded model used for the data analysis is given by^[38]

$$\frac{1}{k(\varphi)} = \left[\frac{1}{k_0} + \frac{1}{4\pi D(\varphi)\rho_{AB}} \right] \left(\frac{1 - \varphi_x}{1 - A_{\text{occl}}(\varphi)} \right) \quad (6)$$

While for low concentrations the linear relationship holds with

$$A_{\text{occl}}(\varphi) = \tilde{A}\varphi = \frac{\rho_B^3}{\rho_C} \left(1 + \frac{3\rho_C(\rho_{AB} + \rho_C)}{2\rho_B\rho_{AB}} \right) \quad (7)$$

our data displayed saturation effects and the the equation

$$A_{\text{occl}}(\varphi) = \tilde{A}\varphi / (1 + \tilde{A}\varphi) \quad (8)$$

was used instead. Both equations are describing the occlusion for ideal spherical particles, where $\rho_{(B)}$ and $\rho_{(AB)}$ describe the radius and diameter of the monomer, respectively.

Determination of the Crowder-Induced Change of the Gibbs Free Energy Gain, $\Delta\Delta G_{\text{fib}}^{\text{crow}}$: Inhibition (or acceleration) of fibrillar growth could either originate from a difference in the fibrillation kinetics, for example,

by blocking of binding sites, or being the result of modified thermodynamics. The plateau value of the ThT assays was connected to the fibrillar content and could be understood as a measure for the thermodynamic equilibrium between free monomers and monomers that were being incorporated into fibrils.^[22] Thermodynamic descriptions, as simple crystallization-like models (CLM), pictured the increment of the total fibrillar mass, Δm_{fib} , as:^[21]

$$\Delta m_{\text{fib}} = \sigma V c_r, \quad (9)$$

where V is the sample volume and c_r the critical concentration of the protein's solubility. The fibrillar growth was therein solely driven by the supersaturation, σ , that could be further approximated by the initial supersaturation, σ_0 , with $\sigma_0 = (c_0 - c_r)/c_r$ and the initial monomer concentration, c_0 . Within this thermodynamic framework, the ratio of the apparent critical concentrations with and without macromolecular crowding, c_r^{crow}/c_r , could be written as:

$$\frac{c_r^{\text{crow}}}{c_r} = \frac{c_0}{c_r} - \frac{\Delta m_{\text{fib}}^{\text{crow}}}{\Delta m_{\text{fib}}} \left(\frac{c_0}{c_r} - 1 \right) \quad (10)$$

where $\Delta m_{\text{fib}}^{\text{crow}}/\Delta m_{\text{fib}}$ is the likewise ratio of the total fibrillar masses, with and without a crowded environment. As the fibrillar mass linearly scales with the ThT-fluorescence, the quotient $\Delta m_{\text{fib}}^{\text{crow}}/\Delta m_{\text{fib}}$ could be safely replaced by $\Delta F_{\text{plateau}}^{\text{crow}}/\Delta F_{\text{plateau}}$ with $\Delta F_{\text{plateau}}$ describing the experimentally determined final plateau (see Equation (1)). Experimental data were carefully corrected for eventual changes of the ThT fluorescence in different buffer conditions using control measurements of unbound ThT in the same conditions. The resulting difference of the Gibbs free energy for the process of fibrillation in different environments is given by

$$\Delta \Delta G_{\text{fibril}}^{\text{crow}}/RT = \ln(c_r^{\text{crow}}/c_r) \quad (11)$$

with R and T the molar gas constant and the absolute temperature, respectively. In case of a reduced solubility due to macromolecular crowding, c_r^{crow}/c_r would be expected to be smaller than 1 and hence, $\Delta \Delta G < 0$. This expectation agreed with simple model descriptions of fibrillar aggregates formed in the presence of crowders. Meisl and coworkers further found $\Delta \Delta G$ to be length independent and to linearly scale with the volume fraction:^[67]

$$\Delta \Delta G_{\text{fibril}}^{\text{crow}}(\varphi)/RT = -\varphi \left[\left(1 + \frac{\rho_1}{\rho_C} \right) - \frac{1}{n_{\text{strand}}} \frac{\rho_1}{\rho_C} \left(1 + \sqrt{n_{\text{strand}}} \frac{\rho_1}{\rho_C} \right) \right] := -\varphi m \quad (12)$$

Hence, the slope m , with $m > 0$ by definition, solely depends on the ratio of the monomer radius versus crowder radius, ρ_1/ρ_C , and the number of strands of the growing fibril, n_{strand} . Deviations from the linear behavior were assigned to the known tendency of PEG molecules to bind to hydrophobic sites of proteins at higher concentrations.^[42,59] Such a concentration dependent binding would compete, for example, against the binding of the fluorescence marker ThT that binds as well preferably to hydrophobic residues of $A\beta$.^[68] Blocking of binding sites would lead to an apparently reduced plateau fluorescence, $\Delta F_{\text{plateau}}^{\text{crow,app}} = \Delta F_{\text{plateau}}^{\text{crow}} (1 - f_{\text{bound}})$. A simple ligand-binding model was used to account for this effect with the fraction $f_{\text{bound}} = 1/(1 + K_d/\varphi^n)$ following the Hill–Langmuir equation, where K_d is the apparent dissociation constant and n the degree of binding cooperativity. Hence, Equations (10)–(12) could be rewritten by a final equation

$$\frac{\Delta F_{\text{plateau}}^{\text{crow,app}}(\varphi)}{\Delta F_{\text{plateau}}(\varphi = 0)} = \frac{e^{\varphi m} - c_0/c_r}{1 - c_0/c_r} \left(1 - \frac{1}{1 + K_d/\varphi^n} \right) \quad (13)$$

which was used as a fitting function to determine m , K_d , and n .

Supporting Information

Supporting Information is available from the Wiley Online Library or from the author.

Acknowledgements

The authors acknowledge funding by the German Science Foundation (DFG) under Project No. 189853844 - TRR 102 “Polymers under multiple constraints” (project B12). The authors thank for the kind experimental support of G. Hause, Martin-Luther-University Halle (electron microscopy) and for the inspiring scientific discussions and experimental support (fluorescence assays) of J. Balbach, Martin-Luther-University Halle.

Open access funding enabled and organized by Projekt DEAL.

Conflict of Interest

The authors declare no conflict of interest.

Data Availability Statement

The data that support the findings of this study are available from the corresponding author upon reasonable request.

Keywords

amyloid fibrillation, PEG, nucleation, amyloid- β , FCS

Received: November 30, 2022

Revised: March 30, 2023

Published online: May 16, 2023

- [1] F. Chiti, C. M. Dobson, *Annu. Rev. Biochem.* **2006**, *75*, 333.
- [2] M. P. Lambert, A. K. Barlow, B. A. Chromy, C. Edwards, R. Freed, M. Liosatos, T. E. Morgan, I. Rozovsky, B. Trommer, K. L. Viola, P. Wals, C. Zhang, C. E. Finch, G. A. Krafft, W. L. Klein, *Proc. Natl. Acad. Sci. U.S.A.* **1998**, *95*, 6448.
- [3] M. Bucciantini, E. Giannoni, F. Chiti, F. Baroni, L. Formigli, J. Zurdo, N. Taddei, G. Ramponi, C. M. Dobson, M. Stefani, *Nature* **2002**, *416*, 507.
- [4] U. Sengupta, A. N. Nilson, R. Kayed, *EBioMedicine* **2016**, *6*, 42.
- [5] A. J. Dear, T. C. T. Michaels, G. Meisl, D. Klenerman, S. Wu, S. Perrett, S. Linse, C. M. Dobson, T. P. J. Knowles, *Proc. Natl. Acad. Sci. U.S.A.* **2020**, *117*, 12087.
- [6] T. C. T. Michaels, A. Šarić, S. Curk, K. Bernfur, P. Arosio, G. Meisl, A. J. Dear, S. I. A. Cohen, C. M. Dobson, M. Vendruscolo, S. Linse, T. P. J. Knowles, *Nat. Chem.* **2020**, *12*, 445.
- [7] K. H. P. Vu, G. H. Blankenburg, L. Lesser-Rojas, C.-F. Chou, *Molecules* **2022**, *27*, 6448.
- [8] P. Cizas, R. Budvytyte, R. Morkuniene, R. Moldovan, M. Broccio, M. Lösche, G. Niaura, G. Valincius, V. Borutaite, *Arch. Biochem. Biophys.* **2010**, *496*, 84.
- [9] M.-C. Lee, W.-C. Yu, Y.-H. Shih, C.-Y. Chen, Z.-H. Guo, S.-J. Huang, J. C. C. Chan, Y.-R. Chen, *Sci. Rep.* **2018**, *8*, 4772.
- [10] P. Seubert, C. Vigo-Pelfrey, F. Esch, M. Lee, H. Dovey, D. Davis, S. Sinha, M. Schioesmacher, J. Whaley, C. Swindlehurst, R. McCormack, R. Wolfert, D. Selkoe, I. Lieberburg, D. Schenk, *Nature* **1992**, *359*, 325.

- [11] A. E. Roher, C. L. Esh, T. A. Kokjohn, E. M. Castaño, G. D. Van Vickle, W. M. Kalback, R. L. Patton, D. C. Luehrs, I. D. Dauts, Y.-M. Kuo, M. R. Emmerling, H. Soares, J. F. Quinn, J. Kaye, D. J. Connor, N. B. Silverberg, C. H. Adler, J. D. Seward, T. G. Beach, M. N. Sabbagh, *Alzheimer's Dementia* **2009**, 5, 18.
- [12] H. Li, J. Wang, Y. Li, X. Chen, W. Zhang, Y. Zhao, G. Liu, J. Pan, *Sensors Actuators B: Chem.* **2022**, 358, 131481.
- [13] A. B. Fulton, *Cell* **1982**, 30, 345.
- [14] S. B. Zimmerman, S. O. Trach, *J. Mol. Biol.* **1991**, 222, 599.
- [15] S. B. Zimmerman, A. P. Minton, *Annu. Rev. Biophys. Biomol. Struct.* **1993**, 22, 27.
- [16] G. G. Glenner, C. W. Wong, *Biochem. Biophys. Res. Commun.* **1984**, 122, 1131.
- [17] C. L. Masters, G. Simms, N. A. Weinman, G. Multhaup, B. L. McDonald, K. Beyreuther, *Proc. Natl. Acad. Sci. U. S. A.* **1985**, 82, 4245.
- [18] S. D. Quinn, P. A. Dalgarno, R. T. Cameron, G. J. Hedley, C. Hacker, J. M. Lucocq, G. S. Baillie, I. D. W. Samuel, J. C. Penedo, *Mol. BioSyst.* **2014**, 10, 34.
- [19] J. D. Harper, P. T. Lansbury, *Annu. Rev. Biochem.* **1997**, 66, 385.
- [20] E. Chatani, N. Yamamoto, *Biophys. Rev.* **2018**, 10, 527.
- [21] R. Crespo, F. A. Rocha, A. M. Damas, P. M. Martins, *J. Biol. Chem.* **2012**, 287, 30585.
- [22] R. Wetzel, *Acc. Chem. Res.* **2006**, 39, 671.
- [23] B. O'Nuallain, S. Shivaprasad, I. Kheterpal, R. Wetzel, *Biochemistry* **2005**, 44, 12709.
- [24] E. Hellstrand, B. Boland, D. M. Walsh, S. Linse, *ACS Chem. Neurosci.* **2010**, 1, 13.
- [25] A. D. Williams, E. Portelius, I. Kheterpal, J.-T. Guo, K. D. Cook, Y. Xu, R. Wetzel, *J. Mol. Biol.* **2004**, 335, 833.
- [26] R. Frankel, M. Törnquist, G. Meisl, O. Hansson, U. Andreasson, H. Zetterberg, K. Blennow, B. Frohm, T. Cedervall, T. P. J. Knowles, T. Leiding, S. Linse, *Commun. Biol.* **2019**, 2, 365.
- [27] A. P. Minton, *Mol. Cell. Biochem.* **1983**, 55, 119.
- [28] A. P. Minton, *Curr. Opin. Struct. Biol.* **2000**, 10, 34.
- [29] I. Kuznetsova, K. Turoverov, V. Uversky, *Int. J. Mol. Sci.* **2014**, 15, 23090.
- [30] R. Vancraenenbroeck, Y. S. Harel, W. Zheng, H. Hofmann, *Proc. Natl. Acad. Sci. U. S. A.* **2019**, 116, 19506.
- [31] D. Hall, A. P. Minton, *Biophys. Chem.* **2002**, 98, 93.
- [32] D. Hall, A. P. Minton, *Biophys. Chem.* **2004**, 107, 299.
- [33] V. N. Uversky, E. M. Cooper, K. S. Bower, J. Li, A. L. Fink, *FEBS Lett.* **2002**, 515, 99.
- [34] D. M. Hatters, A. P. Minton, G. J. Howlett, *J. Biol. Chem.* **2002**, 277, 7824.
- [35] J. Fung, A. A. Darabie, J. McLaurin, *Biochem. Biophys. Res. Commun.* **2005**, 328, 1067.
- [36] Z. Evgrafova, B. Voigt, A. H. Roos, G. Hause, D. Hinderberger, J. Balbach, W. H. Binder, *Phys. Chem. Chem. Phys.* **2019**, 21, 20999.
- [37] A. P. Minton, *Int. J. Biochem.* **1990**, 22, 1063.
- [38] S. S. Andrews, *Phys. Biol.* **2020**, 17, 045001.
- [39] P. S. Vassat, C. F. Culling, *Arch. Pathol.* **1959**, 68, 487.
- [40] A. A. H. Zanjani, N. P. Reynolds, A. Zhang, T. Schilling, R. Mezzenga, J. T. Berryman, *Biophys. J.* **2020**, 118, 2526.
- [41] C. Feuillie, E. Lambert, M. Ewald, M. Azouz, S. Henry, S. Marsaudon, C. Cullin, S. Lecomte, M. Molinari, *Front. Mol. Biosci.* **2020**, 7, 571696.
- [42] M. Biancalana, S. Koide, *Biochim. Biophys. Acta* **2010**, 1804, 1405.
- [43] G. Meisl, X. Yang, C. M. Dobson, S. Linse, T. P. J. Knowles, *Chem. Sci.* **2017**, 8, 4352.
- [44] B. Barz, A. K. Buell, S. Nath, *Chem. Commun.* **2021**, 57, 947.
- [45] Y. Xiao, B. Ma, D. Mcelheny, S. Parthasarathy, F. Long, M. Hoshi, R. Nussinov, Y. Ishii, *Nat. Struct. Mol. Biol.* **2015**, 22, 499.
- [46] A. K. Paravastu, R. D. Leapman, W.-M. Yau, R. Tycko, *Proc. Natl. Acad. Sci. U. S. A.* **2008**, 105, 18349.
- [47] U. Ghosh, K. R. Thurber, W.-M. Yau, R. Tycko, *Proc. Natl. Acad. Sci. U. S. A.* **2021**, 118, e2023089118.
- [48] S. Nag, B. Sarkar, A. Bandyopadhyay, B. Sahoo, V. K. Sreenivasan, M. Kombrabail, C. Muralidharan, S. Maiti, *J. Biol. Chem.* **2011**, 286, 13827.
- [49] M. Schneider, S. Walta, C. Cadek, W. Richtering, D. Willbold, *Sci. Rep.* **2017**, 7, 2154.
- [50] J. J. Mittag, S. Milani, D. M. Walsh, J. O. Rädler, J. J. Mcmanus, *Biochem. Biophys. Res. Commun.* **2014**, 448, 195.
- [51] H. Fatafta, M. Khaled, M. C. Owen, A. Sayyed-Ahmad, B. Strodel, *Proc. Natl. Acad. Sci. U. S. A.* **2021**, 118, e2106210118.
- [52] W. Zheng, M.-Y. Tsai, P. G. Wolynes, *J. Am. Chem. Soc.* **2017**, 139, 16666.
- [53] M. Hashemi, Y. Zhang, Z. Lv, Y. L. Lyubchenko, *Nanoscale Adv.* **2019**, 1, 3892.
- [54] S. I. A. Cohen, M. Vendruscolo, M. E. Welland, C. M. Dobson, E. M. Terentjev, T. P. J. Knowles, *J. Chem. Phys.* **2011**, 135, 065105.
- [55] S. I. A. Cohen, S. Linse, L. M. Luheshi, E. Hellstrand, D. A. White, L. Rajah, D. E. Otzen, M. Vendruscolo, C. M. Dobson, T. P. J. Knowles, *Proc. Natl. Acad. Sci. U. S. A.* **2013**, 110, 9758.
- [56] G. Meisl, X. Yang, E. Hellstrand, B. Frohm, J. B. Kirkegaard, S. I. A. Cohen, C. M. Dobson, S. Linse, T. P. J. Knowles, *Proc. Natl. Acad. Sci. U. S. A.* **2014**, 111, 9384.
- [57] N. V. Dovidchenko, A. V. Glyakina, O. M. Selivanova, E. I. Grigorashvili, M. Y. Suvorina, U. F. Dzhus, A. O. Mikhailina, N. G. Shiliaev, V. V. Marchenkov, A. K. Surin, O. V. Galzitskaya, *J. Struct. Biol.* **2016**, 194, 404.
- [58] C. F. Lee, S. Bird, M. Shaw, L. Jean, D. J. Vaux, *J. Biol. Chem.* **2012**, 287, 38006.
- [59] T. Arakawa, S. N. Timasheff, *Biochemistry* **1985**, 24, 6756.
- [60] S. Kuga, *J. Chromatogr. A* **1981**, 206, 449.
- [61] L. O. Tjernberg, A. Pramanik, S. Björling, P. Thyberg, J. Thyberg, C. Nordstedt, K. D. Berndt, L. Terenius, R. Rigler, *Chem. Biol.* **1999**, 6, 53.
- [62] J. D. Camino, P. Gracia, N. Cremades, *Biophys. Chem.* **2021**, 269, 106520.
- [63] P. Schuck, *Biophys. J.* **2000**, 78, 1606.
- [64] J. Wägele, S. De Sio, B. Voigt, J. Balbach, M. Ott, *Biophys. J.* **2019**, 116, 227.
- [65] L. M. Lauth, B. Voigt, T. Bhatia, L. Machner, J. Balbach, M. Ott, *FEBS Lett.* **2022**, 596, 2928.
- [66] A. M. Berezhkovskii, A. Szabo, *J. Phys. Chem. B* **2016**, 120, 5998.
- [67] R. J. Ellis, A. P. Minton, *Biol. Chem.* **2006**, 387, 485.
- [68] D. Zhao, Y. Chen, Q. Liu, Y. Zhao, Y. Li, *Sci. China: Chem.* **2012**, 55, 112.